Spin-locked scattering of unpolarized light by magnetoelectric coupling

Wenjia Li,[1] Haoran Li,[1] Zhaoqi Jiang,[1] Wenxia Xu,[1] Yang Gao,[2] Shutian Liu,[3] Zheng Zhu,[1] Chunying Guan,[1] Jinhui Shi,[1,*] and Jianlong Liu[1,†]

[1]*Key Laboratory of In-Fiber Integrated Optics of Ministry of Education, College of Physics and Optoelectronic Engineering, Harbin Engineering University, Harbin 150001, China*

[2]*College of Electronic Engineering, Heilongjiang University, Harbin 150080, China*

[3]*School of Physics, Harbin Institute of Technology, Harbin 150001, China*

(Received 27 February 2022; revised 9 October 2022; accepted 17 October 2022; published 1 November 2022)

Unpolarized light is ubiquitous in nature. It does not carry spin angular momentum but it can be converted to partially polarized light with spin angular momentum after scattering. In this work, we demonstrate that the unpolarized light not only possesses a definite spin state after scattering but also induces lateral separation of scattered light with opposite chiralities. Such spin-locked scattering of unpolarized light stems from the inherent property of magnetoelectric coupling of the scatterer. Moreover, the spin-locked scattering for arbitrary linearly polarized light is also investigated and compared with the case of unpolarized light. Our findings can broaden the application range of unpolarized light and open other avenues for spin-related phenomena induced by unpolarized light.

DOI: 10.1103/PhysRevA.106.053501

I. INTRODUCTION

Angular momentum of light plays an indispensable role in modern optics. It is divided into spin angular momentum (SAM) and orbital angular momentum (OAM). SAM is influenced by the polarization state and OAM is dependent on the spatial distribution of the field. Spin-orbit interaction of light refers to the coupling of SAM and OAM of light [1,2]. Spin-locked scattering originates from the spin-orbit interaction of light, which manifests as polarized light with opposite chiralities located in different directions [3–5]. In recent years, there has been a growing interest in spin-locked scattering due to its potential applications in polarization detection, optical metrology, and on-chip optical manipulation [6–10]. In general, spin-locked scattering does not exist for plane waves in conventional media. Nonparaxial optical fields such as evanescent waves and tightly focused beams provide pathways to achieve spin-locked scattering [8,11–15]. In contrast to a conventional medium, bianisotropic media can realize spin-locked scattering for bulk modes based on magnetoelectric coupling [16]. Furthermore, the spin-locked scattering can be induced by the polarized light acting on a bianisotropic particle [17]. Notably, spin-locked scattering may give rise to intriguing phenomena such as asymmetric scattering, spin-controlled unidirectional waveguided modes, and radiation [4,18,19].

Unpolarized light is ubiquitous in nature and consists of polarization states in all directions perpendicular to the propagating direction of the light. Spin-locked scattering under unpolarized light can survive in tightly focused beams and evanescent waves generated by the spin-orbit interaction of light [20,21]. The resulting nonparaxial field stems from the transformation of the wave vector direction, which leads to spin dependent phenomena. Besides, the incident polarization independent spin Hall effect has been proved both analytically and numerically in Ref. [22], in which the reflected beam can be split equally into opposite circular polarizations under unpolarized incidence. The unpolarized light-dependent spin phenomena contain interesting physical mechanisms and can broaden the applicability of the spin-orbit interaction of light to cover optical systems with unpolarized light.

Specially designed particles under unpolarized light may generate unusual dipole moments that can inspire novel physical phenomena. In this paper, we demonstrate that unpolarized light can induce spin-locked scattering by exploiting the magnetoelectric coupling property of the particle. We analyze the intrinsic mechanism of the spin-locked scattering excited by unpolarized light and reveal the relationship between the polarization state of the scattered far field and the dipole moments of the particle. Under an unpolarized incidence, both the transverse spin electric dipole and magnetic dipole of the particle are excited based on magnetoelectric coupling. Particularly, diverse Stokes polarization parameters can be achieved in the near field. In addition, we investigate the spin-locked scattering of arbitrary linearly polarized light and compare with the case of unpolarized light. Our findings offer an alternative route to achieve spin-related phenomena induced by unpolarized incidence, which may broaden the application range of unpolarized light.

II. THEORETICAL MODEL AND REALIZATION

We use a dipole model assuming that the particle solely has electric and magnetic dipole responses. The electric and magnetic dipole moments can be written as

$$\mathbf{p} = (p_x, p_y, p_z)^T, \tag{1}$$

$$\mathbf{m} = (m_x, m_y, m_z)^T. \tag{2}$$

*Corresponding author: shijinhui@hrbeu.edu.cn
†Corresponding author: liujl@hrbeu.edu.cn

In cgs units, the electric field of the scattered far field is given by

$$\mathbf{E}_{\rm sc} = \frac{k_0^2 e^{ik_0 r}}{r}[(\hat{\mathbf{n}} \times \mathbf{p}) \times \hat{\mathbf{n}} - \hat{\mathbf{n}} \times \mathbf{m}], \tag{3}$$

where k_0 is the wave number in free space, r is the distance from the particle center, and $\hat{\mathbf{n}}$ is the unit directional vector. The scattered electric field $\mathbf{E}_{\rm sc}$ can be decomposed into three orthogonal components E_r, E_θ, and E_φ. θ is the elevation angle with respect to the z axis and φ is the azimuthal angle in the x-y plane. In the spherical coordinate system, E_θ and E_φ can be written as follows:

$$E_\theta = \frac{k_0^2 e^{ik_0 r}}{r}[\cos\varphi(m_y + p_x\cos\theta) - \sin\varphi(m_x - p_y\cos\theta) - p_z\sin\theta], \tag{4}$$

$$E_\varphi = \frac{k_0^2 e^{ik_0 r}}{r}[\cos\varphi(p_y - m_x\cos\theta) - \sin\varphi(p_x + m_y\cos\theta) + m_z\sin\theta]. \tag{5}$$

The SAM density $\mathbf{S}$ of the scattered electric field can be expressed as

$$\mathbf{S} \propto \mathrm{Im}[\mathbf{E}_{\rm sc}^* \times \mathbf{E}_{\rm sc}]. \tag{6}$$

The Stokes polarization parameter S_0 is the intensity of the electric field that can be written as

$$S_0 = |\mathbf{E}_{\rm sc}|^2. \tag{7}$$

The Stokes polarization parameter S_3 represents the preponderance of right circularly polarized (RCP) over left circularly polarized (LCP) light. The normalized Stokes polarization parameter S_3/S_0 is related to the normalized SAM density of the scattered field. The normalized Stokes polarization parameter $S_3/S_0 = -1$, 0, and 1 denote left circular, linear, and right circular polarizations, respectively. S_3 of the scattered electric field can be divided into S_{3r}, $S_{3\theta}$, and $S_{3\varphi}$ in the different directions that can be described by

$$S_{3r} = \mathrm{Im}(E_\theta^* E_\varphi - E_\varphi^* E_\theta), \tag{8}$$

$$S_{3\theta} = \mathrm{Im}(E_\varphi^* E_r - E_r^* E_\varphi), \tag{9}$$

$$S_{3\varphi} = \mathrm{Im}(E_r^* E_\theta - E_\theta^* E_r). \tag{10}$$

In the scattered far field, there is only S_{3r} due to the absence of the longitudinal electric field E_r. By inserting Eqs. (4) and (5) into Eq. (8), we obtain

$$\begin{aligned} S_{3r} &= 2\mathrm{Im}(E_\theta^* E_\varphi) \\ &= 2\frac{k_0^4}{r^2}\mathrm{Im}\{[\cos\varphi(m_y^* + p_x^*\cos\theta) \\ &\quad \times -\sin\varphi(m_x^* - p_y^*\cos\theta) - \sin\theta p_z^*] \\ &\quad \times [\cos\varphi(p_y - m_x\cos\theta) \\ &\quad \times -\sin\varphi(p_x + m_y\cos\theta) + \sin\theta m_z]\}. \end{aligned} \tag{11}$$

A particular particle under the illumination of an unpolarized plane wave is shown schematically in Fig. 1(a).

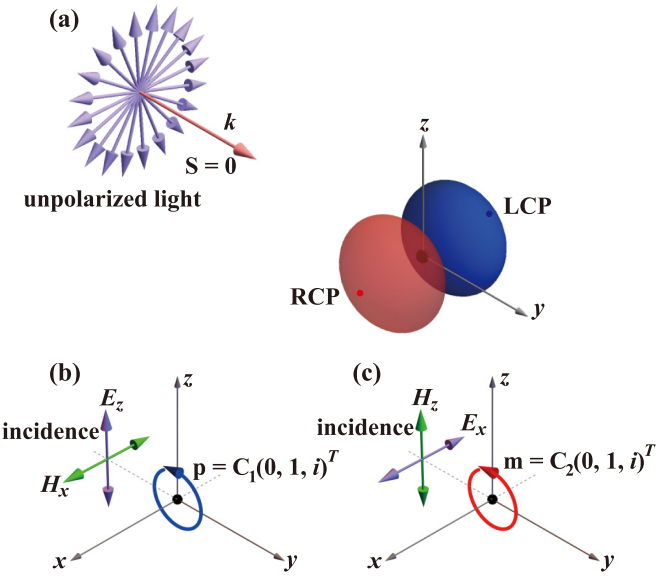

FIG. 1. (a) Schematic of perfect spin-locked scattering by a particle under unpolarized incidence. (b) Illustration of a transverse spin electric dipole. (c) Illustration of a transverse spin magnetic dipole.

The polarized light with opposite chiralities is separated in the scattered field. The RCP and LCP lights are located in opposite lateral directions. The incident unpolarized light propagates along the y axis without a spin state.

Unpolarized light consists of polarization states in all directions perpendicular to the propagating direction. The polarization state of the scattered field under the incidence of unpolarized light is determined by the incoherent superposition of scattered light. Note that the unpolarized light can be considered as an incoherent superposition of two waves with mutually orthogonal polarization states [20]. Therefore, the polarization state of the scattered light under unpolarized light incidence can be obtained by using two incident lights with orthogonal polarizations $\mathbf{E}_{\rm inc}^1 = (0,\ 0,\ 1)^T$ and $\mathbf{E}_{\rm inc}^2 = (1,\ 0,\ 0)^T$. If the two orthogonally polarized lights both produce the same spin splitting, according to the theory of incoherent superposition, a similar phenomenon can also be achieved by using unpolarized light, as shown in Fig. 1(a). In general, spin splitting under the polarized incidence can be achieved by constructing transverse spin dipoles [3,17]. The two incidences are supposed to excite two kinds of ideal transverse spin dipoles as shown in Figs. 1(b) and 1(c), respectively. The ideal transverse spin dipoles can be written as $\mathbf{p} = C_1(0,\ 1,\ i)^T$ and $\mathbf{m} = C_2(0,\ 1,\ i)^T$, which lead to polarized light with opposite chiralities into opposite directions. C_1 and C_2 are arbitrary complex numbers. The longitudinal moments (p_y and m_y) are essential for the transverse spin dipoles, but they are difficult to excite because light is a transverse wave.

Recently, magnetoelectric coupling has attracted increasing attention due to the unusual property in cross induction between electromagnetic fields [23–28]. Particles with magnetoelectric coupling are promising for achieving electric and magnetic transverse spin dipoles due to the available longitudinal dipole moment. In this paper, we propose to exploit the magnetoelectric coupling of the particle to obtain spin-locked scattering of unpolarized light. The particle is a

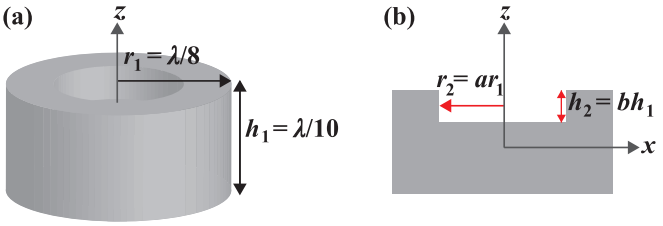

FIG. 2. (a) Schematic of the particle with magnetoelectric coupling. (b) Geometry of the particle in the x-z plane.

nonmagnetic dielectric disk of radius r_1 ($= \lambda/8$), height h_1 ($= \lambda/10$), and relative permittivity $\varepsilon = 40$ with an air hole of radius r_2 ($= ar_1$) and height h_2 ($= bh_1$), as shown in Figs. 2(a) and 2(b). It has been widely employed in magnetoelectric coupling configurations [17,25,26].

Unpolarized incident light propagates along the y axis. Considering the magnetoelectric coupling, the induced dipole moments of the particle can be calculated as

$$\begin{pmatrix} p_x \\ p_y \\ p_z \end{pmatrix} = \begin{pmatrix} \alpha_{ee}^{xx} & 0 & 0 \\ 0 & \alpha_{ee}^{yy} & 0 \\ 0 & 0 & \alpha_{ee}^{zz} \end{pmatrix} \begin{pmatrix} E_x \\ E_y \\ E_z \end{pmatrix} + \begin{pmatrix} 0 & \alpha_{em}^{xy} & 0 \\ \alpha_{em}^{yx} & 0 & 0 \\ 0 & 0 & 0 \end{pmatrix} \begin{pmatrix} H_x \\ H_y \\ H_z \end{pmatrix}, \tag{12}$$

$$\begin{pmatrix} m_x \\ m_y \\ m_z \end{pmatrix} = \begin{pmatrix} \alpha_{mm}^{xx} & 0 & 0 \\ 0 & \alpha_{mm}^{yy} & 0 \\ 0 & 0 & \alpha_{mm}^{zz} \end{pmatrix} \begin{pmatrix} H_x \\ H_y \\ H_z \end{pmatrix} + \begin{pmatrix} 0 & \alpha_{me}^{xy} & 0 \\ \alpha_{me}^{yx} & 0 & 0 \\ 0 & 0 & 0 \end{pmatrix} \begin{pmatrix} E_x \\ E_y \\ E_z \end{pmatrix}, \tag{13}$$

where α_{ee}^{xx}, α_{ee}^{yy}, and α_{ee}^{zz} are the electric polarizabilities in the x, y, and z directions; α_{mm}^{xx}, α_{mm}^{yy}, and α_{mm}^{zz} are the magnetic polarizabilities in the x, y, and z directions; and α_{em}^{xy}, α_{em}^{yx}, α_{me}^{xy}, and α_{me}^{yx} are the polarizabilities of magnetoelectric coupling. According to the symmetry of the particle in the x and y directions, it is deduced that $\alpha_{ee}^{xx} = \alpha_{ee}^{yy}$, $\alpha_{mm}^{xx} = \alpha_{mm}^{yy}$, and $\alpha_{em}^{xy} = \alpha_{me}^{xy} = -\alpha_{em}^{yx} = -\alpha_{me}^{yx}$. In this way, the longitudinal electric dipole (p_y) can be excited by the incident H_x and the longitudinal magnetic dipole (m_y) can be generated by the incident E_x.

For the unpolarized light, we can choose two orthogonal incident fields $\mathbf{E}_{inc}^1 = (0,\ 0,\ 1)^T$ and $\mathbf{E}_{inc}^2 = (1,\ 0,\ 0)^T$ for incoherent superposition. In the two cases, the polarizabilities of the particle can be expressed as $(0, p_y, p_z, m_x, 0, 0)^T$ and $(p_x, 0, 0, 0, m_y, m_z)^T$. The averaged Stokes polarization parameters can be written as

$$S_i^{\mathrm{U}} = \tfrac{1}{2}\left(S_i^1 + S_i^2\right), \tag{14}$$

where S_i ($i = 0,\ 1,\ 2,\ 3$) represent the Stokes polarization parameters of the scattered far field. The superscripts 1 and 2 correspond to the two orthogonally polarized incidences, respectively. The normalized Stokes polarization parameter $S_{3r}^{\mathrm{U}}/S_0^{\mathrm{U}}$ represents the normalized longitudinal SAM density of the scattered field under the unpolarized light, which can be expressed as

$$\begin{aligned} S_{3r}^{\mathrm{U}}/S_0^{\mathrm{U}} \propto \cos\varphi \mathrm{Im}\{&[\sin\varphi(p_y^*\cos\theta - m_x^*) \\ &- p_z^*\sin\theta](p_y - m_x\cos\theta) \\ &+ [m_z\sin\theta - \sin\theta(p_x + m_y\cos\theta)](m_y^* + p_x^*\cos\theta)\}. \end{aligned} \tag{15}$$

It is clear that $S_{3r}^{\mathrm{U}}/S_0^{\mathrm{U}}$ is 0 (linear polarization) at $\varphi = 90^\circ$ and 270° for all θ. It is a necessary condition for the perfect spin-locked scattering in Fig. 1(a).

III. SPIN PROPERTIES IN THE FAR FIELD

We begin the discussion by considering the incidence $\mathbf{E}_{inc}^1 = (0, 0, 1)^T$ to construct the electric transverse spin dipole. The dipole moments of a particle are dependent on its shape and material. The dependency of the dipole moments with the shape of the cylindrical air hole is shown in Figs. 3(a)–3(f) where the magnitudes and phases of the dipole moments provide a direct guide to evaluate the transverse spin dipole. The spin dipole is generated when the magnitudes of p_y and p_z are close to each other, the phase difference between p_y and p_z is $\pi/2$, and m_x is weak. In this case, the spin dipole can be achieved approximatively in the zones marked by stars in Figs. 3(a)–3(f).

We proceed to discuss the incidence with field $\mathbf{E}_{inc}^2 = (1, 0, 0)^T$ to construct the magnetic transverse spin dipole. As is shown in Figs. 4(a)–4(f), the spin dipole occurs in the region marked by stars satisfying $m_z = -im_y$ (green stars) or $m_z = im_y$ (yellow stars) and $p_x = 0$, approximatively. The green and yellow stars correspond to the magnetic spin dipoles with opposite signs. It is worth noting that the electric and magnetic transverse spin dipoles are both excited by utilizing this configuration [Figs. 1(b) and 1(c)]. If the spin-locked scattering field is generated by the unpolarized light, the two spin dipole moments should be in the same direction. Therefore, only areas close to the yellow stars are eligible.

To further evaluate the transverse spin dipole, we define the spin factors P_t and M_t for the electric and magnetic transverse spin dipoles, respectively. For the two orthogonal incidences, the spin factors P_t and M_t can be given by

$$P_t = 2\mathrm{Im}(p_y^* p_z)/(m_x^* m_x + p_y^* p_y + p_z^* p_z), \tag{16}$$

$$M_t = 2\mathrm{Im}(m_y^* m_z)/(p_x^* p_x + m_y^* m_y + m_z^* m_z). \tag{17}$$

The spin factors are ± 1 for the ideal transverse spin dipole. The spin factors P_t and M_t change with a and b [see Figs. 5(a) and 5(b)]. The values of P_t and M_t are both equal to 1, approximatively, at the solid star marker in Figs. 5(a) and 5(b), which means that the electric and magnetic transverse spin dipoles can be excited simultaneously for this structure with such geometric parameters.

Here we investigate the evolution of spin factors P_t and M_t with b at fixed $a = 0.68$ [see Fig. 6(a)]. The solid and dotted curves denote P_t and M_t, respectively. The red point marked in Fig. 6(a) at $b = 0.32$ corresponds to the solid stars shown in Figs. 5(a) and 5(b). The unpolarized incidence satisfies $(S_0,\ S_1,\ S_2,\ S_3) \propto (1,\ 0,\ 0,\ 0)$ [20,22], while the

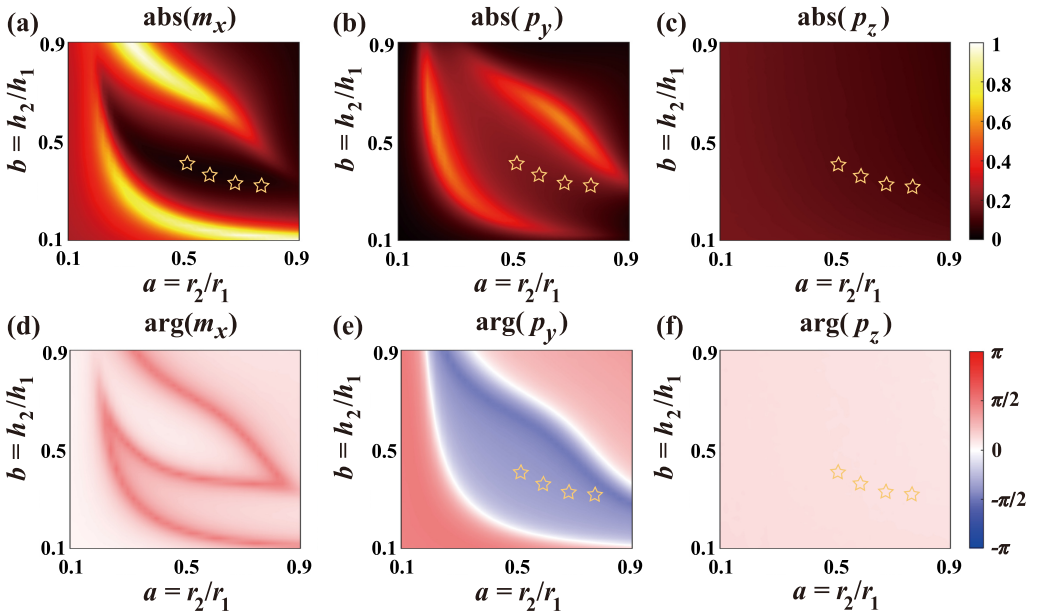

FIG. 3. Dependence of dipole moments on a and b for E_z incidence. (a–c) The magnitudes of the dipole moments m_x, p_y, and p_z. (d–f) The phases of each dipole moment.

polarization comes into being in the scattered light due to the interaction between the light and the particle. To unravel our theory, the distribution of the normalized Stokes polarization parameter $S_{3r}^{\mathrm{U}}/S_0^{\mathrm{U}}$ in the scattered far field at $a = 0.68$ and $b = 0.32$ are shown in Fig. 6(b). The unpolarized incidence can be considered as an incoherent superposition of two orthogonally polarized incidences with the same intensity. Thus S_{3r}^{U} has the additive properties for the two incidences. More importantly, LCP and RCP are equally split in the opposite lateral directions as shown in Fig. 6(b). Such a phenomenon is also known as the giant spin Hall effect of light. To obtain the spin-locked scattering under unpolarized incidence, it is most important to construct the transverse spin dipoles under two orthogonally polarized incidences. The excited transverse spin dipoles lead to the giant spin Hall effect of light for the unpolarized incidence.

IV. SPIN PROPERTIES IN THE NEAR FIELD

Compared with the scattered far field, the scattered near field is more interesting because of the more diverse distributions of the electromagnetic components in the near field.

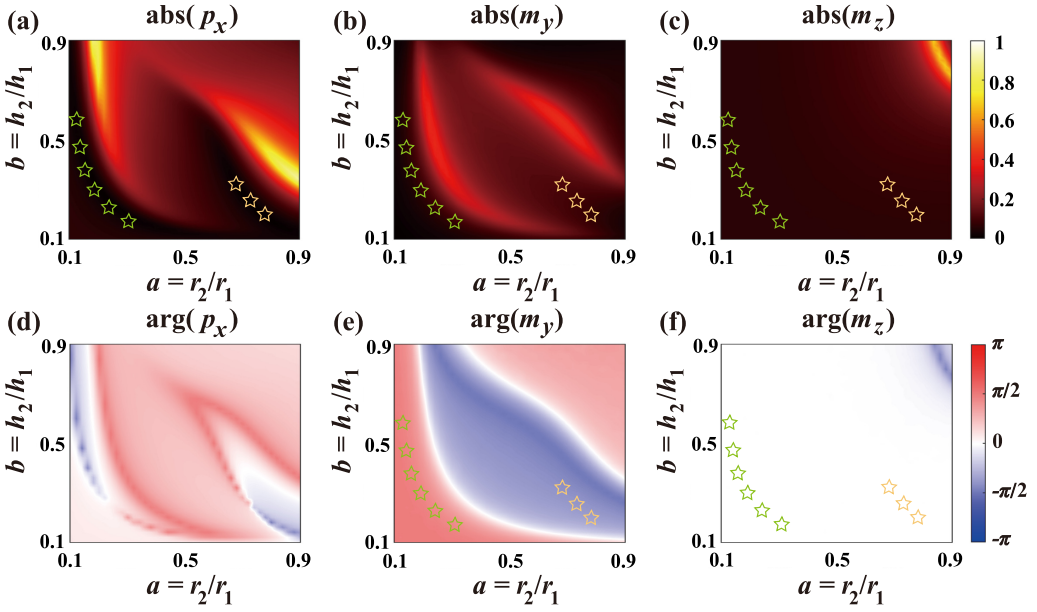

FIG. 4. Dependence of dipole moments on a and b for E_x incidence. (a–c) The magnitudes of the dipole moments p_x, m_y, and m_z. (d–f) The phases of each dipole moment.

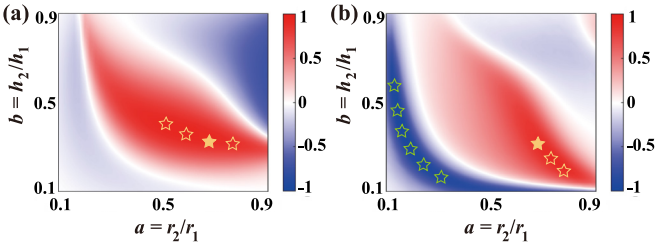

FIG. 5. Dependence of spin factors (a) P_t and (b) M_t on a and b.

In cgs units, the electric field of the scattered near field is given by

$$\mathbf{E}_{\rm sc} \propto \frac{k_0^2}{r}(\hat{\mathbf{n}}\times\mathbf{p})\times\hat{\mathbf{n}} + [3\hat{\mathbf{n}}(\hat{\mathbf{n}}\cdot\mathbf{p}) - \mathbf{p}]\left(\frac{1}{r^3} - \frac{ik_0}{r^2}\right) - \frac{k_0^2}{r}(\hat{\mathbf{n}}\times\mathbf{m})\left(1 - \frac{1}{ik_0 r}\right). \tag{18}$$

In this case, the electric field has transverse and longitudinal components that can be expressed as

$$E_r \propto (1 - ik_0 r)[p_z\cos\theta + (p_x\cos\varphi + p_y\sin\varphi)\sin\theta], \tag{19}$$

$$E_\theta \propto \cos\varphi\left[p_x\left(k_0^2r^2 + ik_0r - 1\right)\cos\theta + k_0 m_y r(i + k_0 r)\right] + \sin\varphi\left[p_y\left(k_0^2r^2 + ik_0r - 1\right)\cos\theta - k_0 m_x r(i + k_0 r)\right] - p_z\left(k_0^2r^2 + ik_0r - 1\right)\sin\theta, \tag{20}$$

$$E_\varphi \propto \cos\varphi\left[p_y\left(k_0^2r^2 + ik_0r - 1\right) - k_0 m_x r(i + k_0 r)\cos\theta\right] - \sin\varphi\left[p_x\left(k_0^2r^2 + ik_0r - 1\right) + k_0 m_y r(i + k_0 r)\cos\theta\right] + k_0 m_z r(i + k_0 r)\sin\theta. \tag{21}$$

It can be inferred that the longitudinal component (E_r) decays faster with propagation distance than the transverse components (E_θ and E_φ). Therefore, the Stokes polarization parameters $S_{3\theta}$ and $S_{3\varphi}$ can only exist in the near field. Considering the ideal electric and magnetic transverse spin dipoles, the dipole moments satisfy $\mathbf{p} = C_1(0, 1, i)^T$ and $\mathbf{m} = C_2(0, 1, i)^T$, respectively. By inserting the dipole moments into Eqs. (20) and (21), the Stokes polarization parameter S_{3r} on the plane of $\theta = 90^\circ$ can be written as

$$S_{3r}^{\rm e} \propto \cos\varphi, \tag{22}$$

$$S_{3r}^{\rm m} \propto \cos\varphi, \tag{23}$$

where the superscripts "e" and "m" correspond to the ideal electric and magnetic transverse spin dipoles, respectively. By inserting $\mathbf{p} = C_1(0, 1, i)^T$ and $\mathbf{m} = C_2(0, 1, i)^T$, respectively, the Stokes polarization parameter $S_{3\theta}$ on the plane of $\theta = 90^\circ$ can be written as

$$S_{3\theta}^{\rm e} \propto -\sin\varphi\cos\varphi, \tag{24}$$

$$S_{3\theta}^{\rm m} = 0. \tag{25}$$

The electric and magnetic transverse spin dipoles will generate corresponding spin properties in the electric and magnetic fields. The magnetic field of the scattered near field can be written as

$$\mathbf{H}_{\rm sc} \propto \frac{k_0^2}{r}(\hat{\mathbf{n}}\times\mathbf{m})\times\hat{\mathbf{n}} + [3\hat{\mathbf{n}}(\hat{\mathbf{n}}\cdot\mathbf{m}) - \mathbf{m}]\left(\frac{1}{r^3} - \frac{ik_0}{r^2}\right) + \frac{k_0^2}{r}(\hat{\mathbf{n}}\times\mathbf{p})\left(1 - \frac{1}{ik_0 r}\right). \tag{26}$$

The longitudinal and transverse components of the magnetic field can be expressed as

$$H_r \propto (1 - ik_0 r)[m_z\cos\theta + (m_x\cos\varphi + m_y\sin\varphi)\sin\theta], \tag{27}$$

$$H_\theta \propto \cos\varphi\left[-m_x\left(k_0^2r^2 + ik_0r - 1\right)\cos\theta + k_0 p_y r(i + k_0 r)\right] - \sin\varphi\left[m_y\left(k_0^2r^2 + ik_0r - 1\right)\cos\theta + k_0 p_x r(i + k_0 r)\right] + m_z\left(k_0^2r^2 + ik_0r - 1\right)\sin\theta, \tag{28}$$

$$H_\varphi \propto \cos\varphi\left[m_y\left(k_0^2r^2 + ik_0r - 1\right) + k_0 p_x r(i + k_0 r)\cos\theta\right] - \sin\varphi\left[m_x\left(k_0^2r^2 + ik_0r - 1\right) - k_0 p_y r(i + k_0 r)\cos\theta\right] - k_0 p_z r(i + k_0 r)\sin\theta. \tag{29}$$

The expression of Stokes polarization parameters of the magnetic field analogous to that of the electric field can be presented by

$$S_{3r}^{\rm H} = {\rm Im}(H_\theta^* H_\varphi - H_\varphi^* H_\theta), \tag{30}$$

$$S_{3\theta}^{\rm H} = {\rm Im}(H_\varphi^* H_r - H_r^* H_\varphi), \tag{31}$$

$$S_{3\varphi}^{\rm H} = {\rm Im}(H_r^* H_\theta - H_\theta^* H_r). \tag{32}$$

When $\theta = 90^\circ$, the Stokes polarization parameters $S_{3r}^{\rm H}$ and $S_{3\theta}^{\rm H}$ for the ideal electric and magnetic transverse spin dipoles

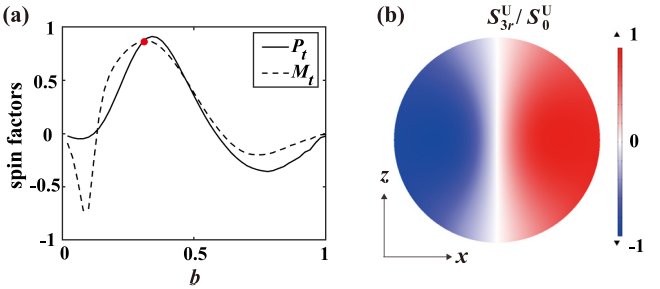

FIG. 6. (a) Evolution of spin factors with b at $a = 0.68$. (b) Distributions of the normalized Stokes polarization parameter $S_{3r}^{\rm U}/S_0^{\rm U}$ in scattered far field at $a = 0.68$ and $b = 0.32$.

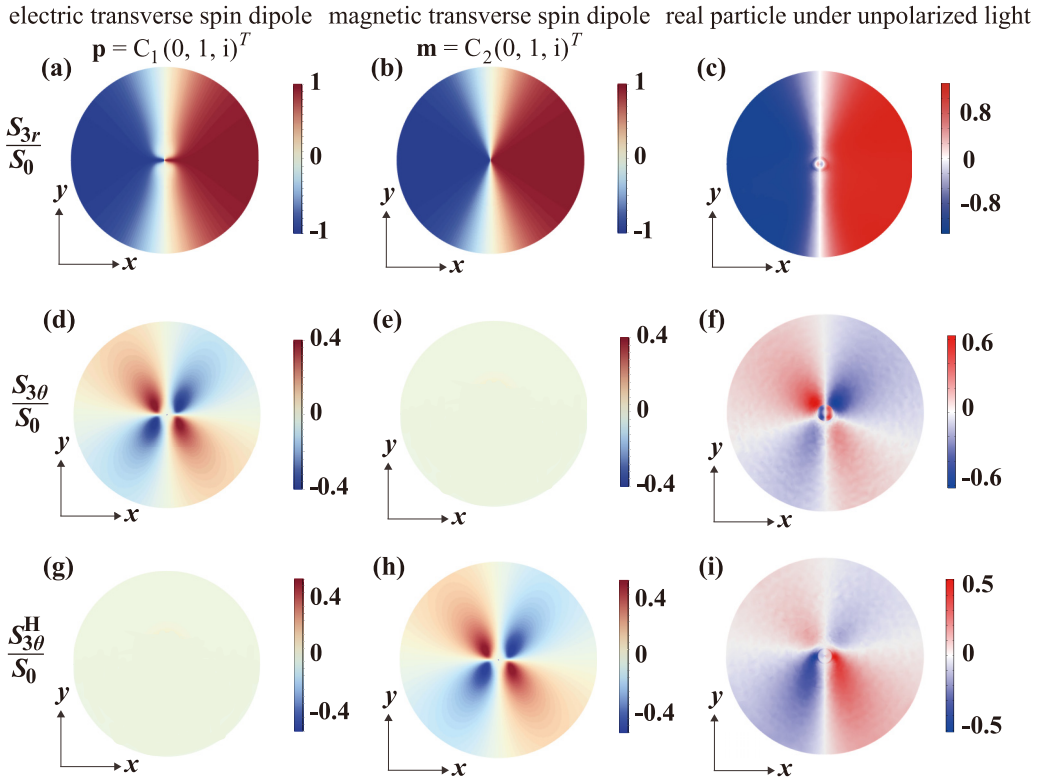

FIG. 7. Distributions of the normalized Stokes polarization parameters S_{3r}/S_0 for (a) the ideal electric transverse spin dipoles, (b) the ideal magnetic transverse spin dipoles, and (c) the real particle on the plane of $\theta = 90°$. Distributions of the normalized Stokes polarization parameters $S_{3\theta}/S_0$ for (d) the ideal electric transverse spin dipoles, (e) the ideal magnetic transverse spin dipoles, and (f) the real particle under unpolarized light. Distributions of the normalized Stokes polarization parameters $S^{\mathrm{H}}_{3\theta}/S_0$ for (g) the ideal electric transverse spin dipoles, (h) the ideal magnetic transverse spin dipoles, and (i) the real particle under unpolarized light.

are given by

$$S^{\mathrm{He}}_{3r} \propto \cos\varphi, \tag{33}$$

$$S^{\mathrm{Hm}}_{3r} \propto \cos\varphi, \tag{34}$$

$$S^{\mathrm{He}}_{3\theta}=0, \tag{35}$$

$$S^{\mathrm{Hm}}_{3\theta} \propto -\sin\varphi\cos\varphi. \tag{36}$$

It is clear that the Stokes polarization parameters S_{3r} for the electric and magnetic fields have the same distributions at $\theta = 90°$. Figures 7(a) and 7(b) show the distributions of S_{3r}/S_0 on the plane of $\theta = 90°$ for ideal electric and magnetic transverse spin dipoles [$\mathbf{p} = C_1(0, 1, i)^T$, $\mathbf{m} = C_2(0, 1, i)^T$], respectively. Figures 7(d) and 7(e) depict the distributions of $S_{3\theta}/S_0$ for the ideal electric and magnetic transverse spin dipoles. It is shown that $S_{3\theta}/S_0$ gradually decreases with the increasing of the propagation distance, which is essentially different from S_{3r}/S_0. Figure 7(e) also reveals that $S_{3\theta}/S_0$ is zero on the plane of $\theta = 90°$ for a magnetic transverse spin dipole, which is in accord with Eq. (25). It is worth noting that the distribution of $S^{\mathrm{H}}_{3\theta}/S_0$ for the magnetic (electric) transverse spin dipoles is the same as the distribution of $S_{3\theta}/S_0$ for the electric (magnetic) transverse spin dipoles. The distributions of $S^{\mathrm{H}}_{3\theta}/S_0$ for the ideal electric and magnetic transverse spin dipoles are shown in Figs. 7(g) and 7(h). Figures 7(c), 7(f), and 7(i) present the distribution of S_{3r}/S_0, $S_{3\theta}/S_0$, and $S^{\mathrm{H}}_{3\theta}/S_0$ for the real particle with $a = 0.68$ and $b = 0.32$ when it is illuminated by unpolarized light. They are almost the same as the incoherent superposition of the two transverse spin dipoles. The error stems from the fact that the unpolarized light not only excites the ideal transverse spin dipoles, but also other components.

V. COMPARISON WITH LINEAR POLARIZATION EXCITATIONS

To exemplarily demonstrate the spin-locked scattering, we move to the case of arbitrary linearly polarized incidence which refers to the linearly polarized light with arbitrary polarization directions. Similar to the unpolarized incidence, the arbitrary linearly polarized incidence can be regarded as a combination of the two orthogonally polarized incidences. The spin-locked scattering under the unpolarized light can be considered as the incoherent superposition result under the two orthogonally polarized incidences, whereas the spin-locked scattering under the arbitrary linearly polarized incidence corresponds to the result of the coherent superposition result. The arbitrary linearly polarized incidence can be decomposed into two orthogonally polarized incidences $\mathbf{E}^1_{\mathrm{inc}} = (0, 0, 1)^T$ and $\mathbf{E}^2_{\mathrm{inc}} = (1, 0, 0)^T$. Assuming the electric transverse spin dipole moment $\mathbf{p} = C_1(0, 1, i)^T$ and magnetic transverse spin dipole moment $\mathbf{m} = C_2(0, 1, i)^T$ are excited by the orthogonally polarized incidences, we substitute the

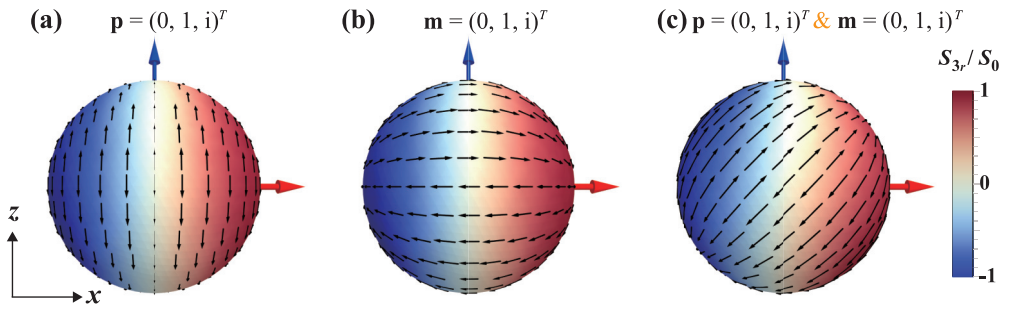

FIG. 8. Distributions of S_{3r}/S_0 in scattered far field at $a = 0.68$ and $b = 0.32$ for incident polarization direction (a) 0°, (b) 30°, (c) 60°, (d) 90°, (e) 120°, and (f) 150° with respect to the x axis.

dipole moments into Eq. (11) that can be written as

$$S_{3r} \propto \mathrm{Im}\{\cos\varphi[(i\sin\theta - \sin\varphi\cos\theta)C_2^* C_2 + (\sin\varphi\cos\theta + i\sin\theta)C_1^* C_1] + \cos^2\varphi C_2^* C_1 - (\sin^2\theta + \sin^2\varphi\cos^2\theta)C_1^* C_2\}. \quad (37)$$

As mentioned above, linear polarization at $\varphi = 90^\circ$ and 270° is the necessary condition for the perfect spin-locked scattering. By substituting $\varphi = 90^\circ$ and 270° into the above formula, the condition for the perfect spin-locked scattering under arbitrary linearly polarized incidence is given by

$$S_{3r} \propto \mathrm{Im}(C_1^* C_2) = 0. \quad (38)$$

It can be formulated as $\arg(C_1) = \arg(C_2) + 2\pi n$, where n is an integer. It means that the two orthogonally polarized fields should induce the electric and magnetic transverse spin dipole moments independently and the phase difference between them should be zero. Figures 8(a) and 8(b) present the distributions of S_{3r}/S_0 in the scattered far field for the ideal spin dipoles with $C_1 = C_2 = 1$. The arrows denote the major axis of the polarization ellipse. The same spin-locked scattering is achieved for the two incidences and there is no phase difference between scattered fields on the *yoz* plane. The coherent superposition of scattered farfields will exhibit separation of light with opposite chiralities as shown in Fig. 8(c).

Then we investigate the performance of the designed particle in spin-locked scattering for arbitrary linearly polarized incidence. The distributions of S_{3r}/S_0 in the scattered far field for incident polarization direction 0°, 30°, 60°, 90°, 120°, and 150° with respect to the x axis are depicted in Figs. 9(a)–9(f). The particle with $a = 0.68$ and $b = 0.32$ is chosen. Interestingly, the scattered light with opposite chiralities is almost split into lateral opposite directions regardless of the incident polarization directions. However, the interface between opposite chiralities is not always located on the *yoz* plane. It originates from the phase difference between the electric and magnetic transverse spin dipole moments. In addition, extra dipole moments may be excited which could also affect the polarization distribution in the scattering far field.

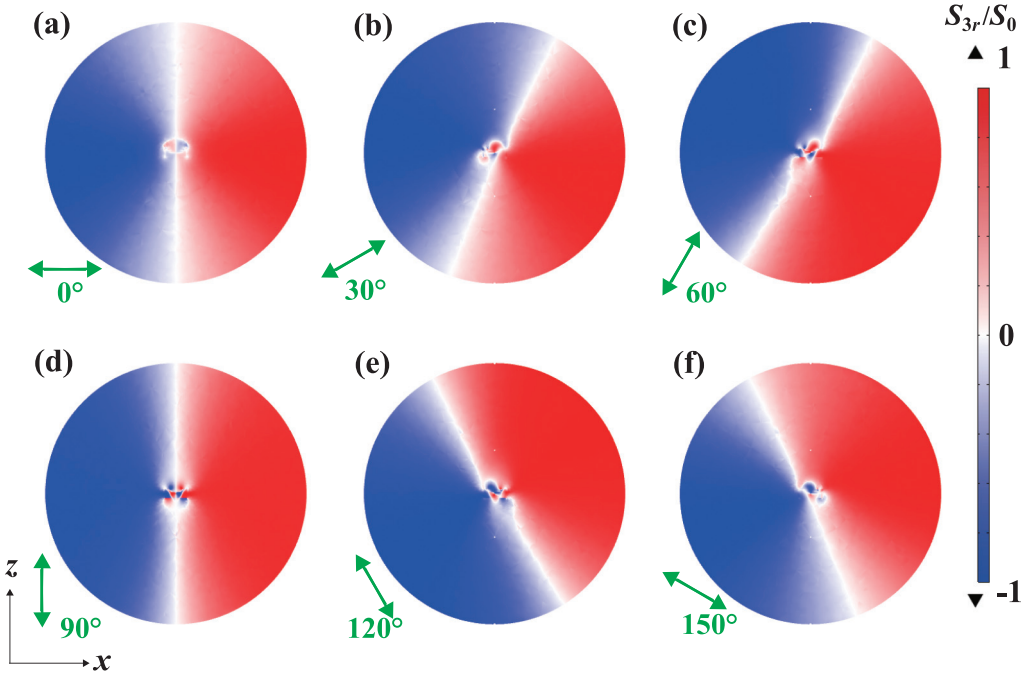

FIG. 9. Distributions of S_{3r}/S_0 in scattered far field for (a) $\mathbf{p} = (0, 1, i)^T$, (b) $\mathbf{m} = (0, 1, i)^T$, and (c) $\mathbf{p} = (0, 1, i)^T$ and $\mathbf{m} = (0, 1, i)^T$.

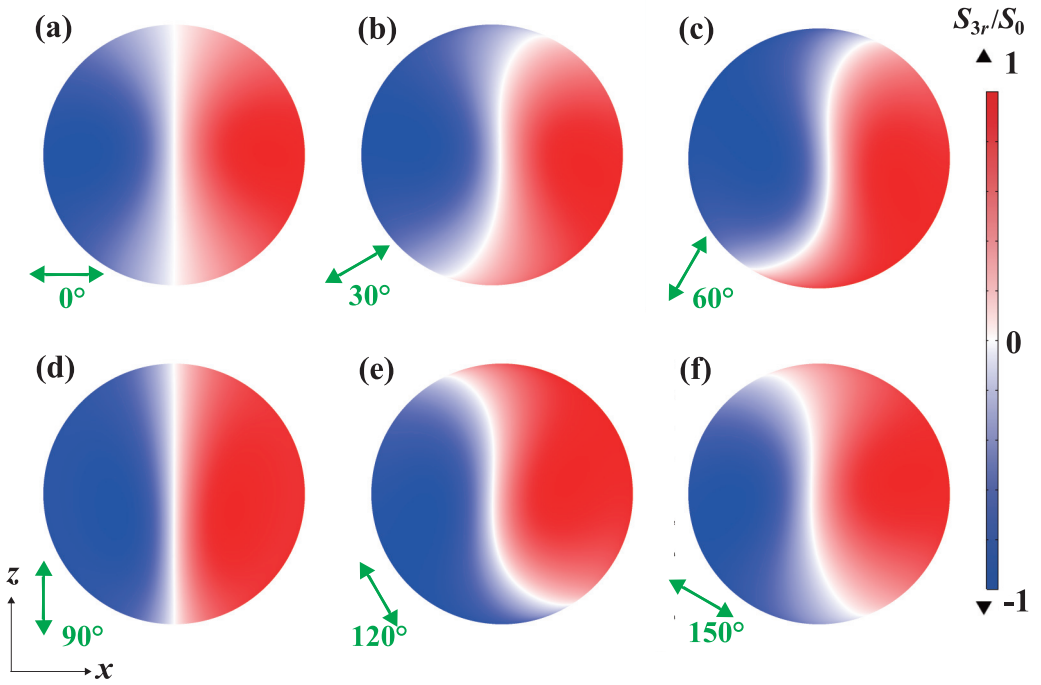

FIG. 10. Distributions of S_{3r}/S_0 in scattered near field at $a = 0.68$ and $b = 0.32$ for incident polarization direction (a) 0 °, (b) 30 °, (c) 60 °, (d) 90 °, (e) 120 °, and (f) 150 ° with respect to the x axis.

Last, we check the spin-locked scattering in the near field for linearly polarized incidence. Figures 10(a)–10(f) depict the distributions of S_{3r}/S_0 on the plane of $\theta = 90°$ for the real particle with $a = 0.68$ and $b = 0.32$ for incident polarization direction 0 °, 30 °, 60 °, 90 °, 120 °, and 150 ° with respect to the x axis. The distributions are basically similar to those in the far field shown in Figs. 9(a)–9(f). It means that the scattered light with opposite chiralities is almost split into lateral opposite directions in both near and far fields regardless of the incident polarization directions.

VI. CONCLUSION

In conclusion, we have discovered an intriguing spin-locked scattering of unpolarized light based on magnetoelectric coupling of the particle and revealed a subtle connection between transverse spin dipole and the spin Hall effect of light which originate from the spin-orbit interaction of light. It is shown that the electric and magnetic transverse spin dipoles can be achieved simultaneously by utilizing the particles with magnetoelectric coupling properties. Furthermore, we reveal the spin properties in the far field and near field. Notably, the condition to achieve the spin-locked scattering for arbitrary linearly polarized light is more severe than that for unpolarized light due to the different superposition manners of the orthogonally polarized light. There must be no phase difference between the excited transverse spin dipoles for the case of arbitrary linearly polarized light. The present study offers a promising avenue for spin-related phenomena by unpolarized light, which is conducive to exploring novel mechanisms of interaction between unpolarized light and particles.

ACKNOWLEDGMENTS

This work was supported by the National Natural Science Foundation of China (Grants No. 12204126, No. 12074087, No. 11874132, and No. U1931121), the Natural Science Foundation of Heilongjiang Province in China (Grant No. LH2021A008), the 111 Project of Harbin Engineering University (Grant No. B13015), and Fundamental Research Funds for the Central Universities (Grants No. 3072022TS2505, No. 3072022TS2509, and No. 3072022TS2501).

[1] K. Y. Bliokh, F. J. Rodriguez-Fortuno, F. Nori, and A. V. Zayats, Nat. Photonics **9**, 796 (2015).
[2] K. Y. Bliokh, D. Smirnova, and F. Nori, Science **348**, 1448 (2015).
[3] S. Nechayev, M. Neugebauer, M. Vorndran, G. Leuchs, and P. Banzer, Phys. Rev. Lett. **121**, 243903 (2018).
[4] M. Neugebauer, P. Wozniak, A. Bag, G. Leuchs, and P. Banzer, Nat. Commun. **7**, 11286 (2016).
[5] B. le Feber, N. Rotenberg, and L. Kuipers, Nat. Commun. **6**, 6695 (2015).
[6] P. Banzer, M. Neugebauer, A. Aiello, C. Marquardt, N. Lindlein, T. Bauer, and G. Leuchs, J. Eur. Opt. Soc., Rapid Publ. **8**, 13032 (2013).
[7] F. Cardano and L. Marrucci, Nat. Photonics **15**, 72 (2021).
[8] M. Neugebauer, T. Bauer, A. Aiello, and P. Banzer, Phys. Rev. Lett. **114**, 063901 (2015).

[9] M. Neugebauer, S. Nechayev, M. Vorndran, G. Leuchs, and P. Banzer, Nano Lett. **19**, 422 (2019).
[10] O. G. Rodriguez-Herrera, D. Lara, K. Y. Bliokh, E. A. Ostrovskaya, and C. Dainty, Phys. Rev. Lett. **104**, 253601 (2010).
[11] K. Y. Bliokh and F. Nori, Phys. Rev. A **85**, 061801(R) (2012).
[12] A. Canaguier-Durand and C. Genet, Phys. Rev. A **89**, 033841 (2014).
[13] Z. Shao, J. Zhu, Y. Chen, Y. Zhang, and S. Yu, Nat. Commun. **9**, 926 (2018).
[14] D. O'Connor, P. Ginzburg, F. J. Rodriguez-Fortuno, G. A. Wurtz, and A. V. Zayats, Nat. Commun. **5**, 5327 (2014).
[15] A. Aiello, P. Banzer, M. Neugebauer, and G. Leuchs, Nat. Photonics **9**, 789 (2015).
[16] L. Peng, L. F. Duan, K. W. Wang, F. Gao, L. Zhang, G. F. Wang, Y. H. Yang, H. S. Chen, and S. Zhang, Nat. Photonics **13**, 878 (2019).
[17] W. Li, J. Shi, C. Guan, Z. Zhu, Y. Gao, S. Liu, and J. Liu, Phys. Rev. B **104**, 235418 (2021).
[18] F. J. Rodriguez-Fortuno, G. Marino, P. Ginzburg, D. O'Connor, A. Martinez, G. A. Wurtz, and A. V. Zayats, Science **340**, 328 (2013).
[19] P. Shi, L. P. Du, C. C. Li, A. V. Zayats, and X. C. Yuan, Proc. Natl. Acad. Sci. U. S. A. **118**, e2018816118 (2021).
[20] J. S. Eismann, L. H. Nicholls, D. J. Roth, M. A. Alonso, P. Banzer, F. J. Rodriguez-Fortuno, A. V. Zayats, F. Nori, and K. Y. Bliokh, Nat. Photonics **15**, 156 (2021).
[21] Y. H. Chen, F. Wang, Z. Dong, Y. J. Cai, A. Norrman, J. J. Gil, A. T. Friberg, and T. Setala, Phys. Rev. A **104**, 013516 (2021).
[22] M. Kim, D. Lee, and J. Rho, Laser Photonics Rev. **15**, 2100138 (2021).
[23] J. Vehmas, Y. Ra'di, A. O. Karilainen, and S. A. Tretyakov, IEEE Trans. Antennas Propag. **61**, 3747 (2013).
[24] R. Alaee, M. Albooyeh, M. Yazdi, N. Komjani, C. Simovski, F. Lederer, and C. Rockstuhl, Phys. Rev. B **91**, 115119 (2015).
[25] R. Alaee, M. Albooyeh, A. Rahimzadegan, M. S. Mirmoosa, Y. S. Kivshar, and C. Rockstuhl, Phys. Rev. B **92**, 245130 (2015).
[26] D. A. Bobylev, D. A. Smirnova, and M. A. Gorlach, Laser Photonics Rev. **15**, 1900392 (2021).
[27] D. V. Zhirihin, S. V. Li, D. Y. Sokolov, A. P. Slobozhanyuk, M. A. Gorlach, and A. B. Khanikaev, Opt. Lett. **44**, 1694 (2019).
[28] W. Li, J. Liu, Y. Gao, K. Zhou, and S. Liu, Phys. Rev. A **102**, 063527 (2020).